



# Construction of Hollow H-CuS/NiS<sub>2</sub>@CuS S-Scheme Heterostructure Photocatalyst with an Excellent Hydrogen Evolution Performance

Tao Zhou, Junzi Li, Xu Han, Yingyu Song, Menglong Liu, Jialiang Liu, Wen-Wen He,\*  
Thamraa AlShahrani, and Shengqian Ma\*

Heterojunction engineering is regarded as one of the most efficacious means to enhance the hydrogen evolution performance of photocatalysts. In this research, bimetal MOF-74 is grown on hollow Cu<sub>7</sub>S<sub>4</sub>, and after vulcanization, H-CuS/NiS<sub>2</sub>@CuS is obtained to form heterostructures. The experimental results indicate that the synthesized H-CuS/NiS<sub>2</sub>@CuS has an outstanding photocatalytic hydrogen evolution rate of 17.66 mmol g<sup>-1</sup> h<sup>-1</sup>, and its photocatalytic hydrogen evolution performance is much higher than that of

single transition metal sulfide. Within the S-scheme heterojunction, the interfacial electric field causes a significant accumulation of photoelectrons on the conduction band of NiS<sub>2</sub>. Thus, it can maintain a high reducing property in the hydrogen evolution reaction and remarkably boosts the separation efficiency of photoelectrons and holes. This research offers a feasible scheme for the synthesis of highly efficient heterojunction photocatalysts.

## 1. Introduction

Energy shortages caused by the overuse of fossil fuels become significant challenges to economic development all over the world. The evolution of energy sources turns out to be an urgent task.<sup>[1–4]</sup> Hydrogen energy is regarded as an excellent alternative energy source due to its high energy density and nonpolluting combustion characteristics.<sup>[5–7]</sup> Following Fujishima and Honda's pioneering work on the photolysis reaction of water in 1972, photocatalytic water decomposition to produce hydrogen was recognized as a clean and efficient technology for converting solar energy into

hydrogen. However, the utilization rate of solar energy is relatively low throughout the existing photocatalyst study field.<sup>[8–11]</sup> Hence, it is essential to design and fabricate photocatalysts with high efficiency.

Metal sulfide (MSs), as a semiconductor material, has the characteristics of good photosensitivity, high conductivity, and excellent photoelectrochemical stability, being a promising photocatalyst in hydrogen evolution reaction (HER).<sup>[12]</sup> However, the photocatalytic activity of solid structure MSs is often limited because of the shortage of low-incident photon absorption, high carrier recombination, insufficient catalytic active sites, and slow charge transfer. The development of hollow structure MSs alleviates these limitations. Compared to solid nanostructured catalysts, semiconductors with unique hollow nanostructured characteristics are more suitable for photocatalysis.<sup>[13]</sup> In 2024, Ding and Yang et al.<sup>[14]</sup> prepared a series of hollow sulfides materials, the average hydrogen evolution rate of these materials was 4.2 times higher than that of the conventional sulfide. The unique hollow structure can fully expose the active site of the reaction, with the merit of improvement in light absorption, making this material excellent photocatalytic hydrogen evolution performance.<sup>[15]</sup>


CuS is a popular material in the field of photocatalytic hydrogen evolution due to its additional absorption band in the near-infrared region (NIR) and narrow-bandgap p-type semiconductor structures. The rapid recombination of CuS photogenerated electron-hole (e-h) pairs limits the development and application of this promising semiconductor material. The construction of heterojunction between CuS and other semiconductors can effectively solve this problem. In 2024, Lian et al.<sup>[16]</sup> constructed a p-n heterojunction by combining CuS with ZnIn<sub>2</sub>S<sub>4</sub>. The recombination of photogenerated electrons and holes has been effectively inhibited, making the material excellent photocatalytic hydrogen evolution performance. In the same year, Zhao et al.<sup>[17]</sup> used CuS to construct plasma p-n heterojunctions to improve the photocatalytic overall water-


T. Zhou, X. Han, Y. Song, M. Liu, J. Liu, W.-W. He  
School of Chemistry and Life Science  
Advanced Institute of Materials Science  
Changchun University of Technology  
Changchun 130012, China  
E-mail: heww@ccut.edu.cn

J. Li  
Dalton Academy  
The Affiliated High School of Peking University  
Beijing 100190, China

S. Ma  
Department of Chemistry  
University of North Texas  
1508 W. Mulberry St., Denton, TX 76201, USA  
E-mail: Shengqian.Ma@unt.edu

T. AlShahrani  
Department of Physics  
College of Science  
Princess Nourah bint Abdulrahman University  
Riyadh 11564, Saudi Arabia

 Supporting information for this article is available on the WWW under <https://doi.org/10.1002/ceur.202500073>

 © 2025 The Author(s). ChemistryEurope published by Chemistry Europe and Wiley-VCH GmbH. This is an open access article under the terms of the Creative Commons Attribution License, which permits use, distribution and reproduction in any medium, provided the original work is properly cited.



splitting performance driven by infrared light. Therefore, hollow CuS was selected as the carrier to prepare a composite material, which can provide more active sites for the reaction while maintaining the advantages of CuS in light absorption.

MOF-derived metal sulfides are excellent candidate materials for constructing heterojunction photocatalysts.<sup>[18,19]</sup> The transition metal sulfides derived from MOF can not only retain the atom arrangement of the precursor, but also offer a large specific surface area and more reactive sites, so as to promote the reaction. Hollow CuS has good light absorption ability, and the combination with MOF-derived sulfide can construct heterostructures, which enables an effective separation of photogenerated electrons and holes. The shared S atom can enhance the interaction between the two semiconductor materials while establishing an electron transfer channel, which is conducive to photoelectron transfer, improving the utilization rate of photogenerated electrons.<sup>[20,21]</sup> Therefore, we propose to prepare a composite photocatalyst with a heterogeneous structure by growing MOF-derived sulfide on hollow CuS, so as to realize efficient photocatalytic hydrogen production.

Herein, CuS with hollow structure (H-CuS) has been successfully prepared and loaded with MOF-derived NiS<sub>2</sub> and CuS nano-sheets. The photocatalytic hydrogen production of H-CuS/NiS<sub>2</sub>@CuS composite can reach 17.66 mmol g<sup>-1</sup> h<sup>-1</sup>, and it still has excellent hydrogen evolution performance after four cycle stability tests, indicating that the material has good cycle stability. The mechanism and kinetic behavior of this photocatalyst were further studied by XPS and a series of photochemical experiments. The results show that the electron transfer mechanism of the composite is a typical S-scheme heterostructure. Under the electric field force of the S-scheme heterojunction interface electric field (IEF), the electrons accumulate in the NiS<sub>2</sub> conduction band, which makes them high reducibility in HER, and effectively improves the separation efficiency of e-h pairs. This research offers a feasible idea for the synthesis of heterojunction photocatalysts with outstanding hydrogen evolution performance.

## 2. Results and Discussion

### 2.1. Structure and Characterization of Materials

We first synthesized the 14-pod Cu<sub>2</sub>O precursor by solvothermal method at 100 °C. Subsequently, Cu<sub>2</sub>O was vulcanized to form a Cu<sub>2</sub>O@Cu<sub>7</sub>S<sub>4</sub> core-shell structure using Na<sub>2</sub>S as the sulfur source at 0 °C. The resulting composite was then immersed in ammonia for 2 days to dissolve the Cu<sub>2</sub>O inside to form a Cu<sub>7</sub>S<sub>4</sub> shell with a hollow structure.<sup>[22]</sup> Then, the bimetallic MOF-74 was grown on the surface of the hollow Cu<sub>7</sub>S<sub>4</sub> using solvothermal method at a temperature of 150 °C.<sup>[23–26]</sup> Finally, the H-CuS/NiS<sub>2</sub>@CuS composite was formed by further sulfurization with thioacetamide at 150 °C. In the composite materials, S-scheme heterojunction was constructed. The flow chart of the material preparation is illustrated in **Figure 1**. To prove the integrity of the synthesized materials, the photocatalysts were tested respectively by means of FT-IR and PXRD. As illustrated in Figure S1 (Supporting Information), the Cu<sub>2</sub>O precursor was successfully synthesized.<sup>[22]</sup> As illustrated in **Figure 2a**, the diffraction peak of Cu<sub>7</sub>S<sub>4</sub> matches well with the standard card, which proves the successful synthesis of Cu<sub>7</sub>S<sub>4</sub>. After growing the bimetallic MOF-74 on it, the diffraction peaks of Cu<sub>7</sub>S<sub>4</sub> and MOF-74 did not weaken, indicating that Cu<sub>7</sub>S<sub>4</sub> maintained a good crystal structure when combined with MOF-74.<sup>[23,24]</sup> As illustrated in Figure S2 (Supporting Information), FT-IR shows that the peaks of MOF-74 are consistent with those reported in the literature. After sulfurization with thioacetamide, the diffraction peak belonging to Cu<sub>7</sub>S<sub>4</sub> disappeared, and the diffraction peak belonging to CuS appeared as illustrated in Figure 2b, indicating that during the sulfidation of Cu<sub>7</sub>S<sub>4</sub>, Cu<sup>+</sup> was oxidized to Cu<sup>2+</sup> and further sulfurized to CuS. The small peaks at 35, 38, 45, 53, 58, and 61° were the diffraction peaks of NiS<sub>2</sub>.<sup>[27,28]</sup> Based on the previous results, a composite composed of CuS and NiS<sub>2</sub> has been successfully synthesized.

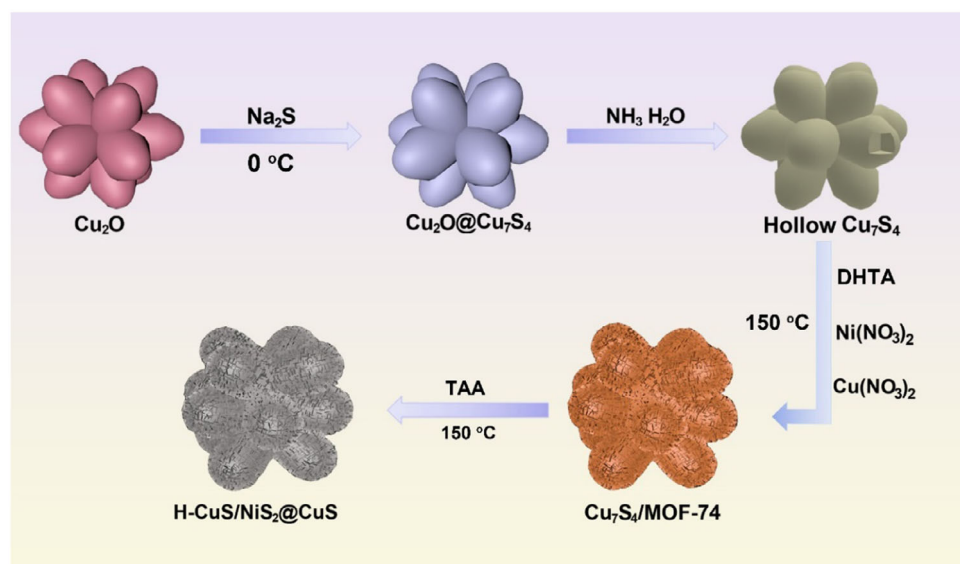


**Figure 1.** Schematic illustration of the synthesis procedure of H-CuS/NiS<sub>2</sub>@CuS. DHTA is 2,5-dihydroxyterephthalic acid. TAA is thioacetamide.

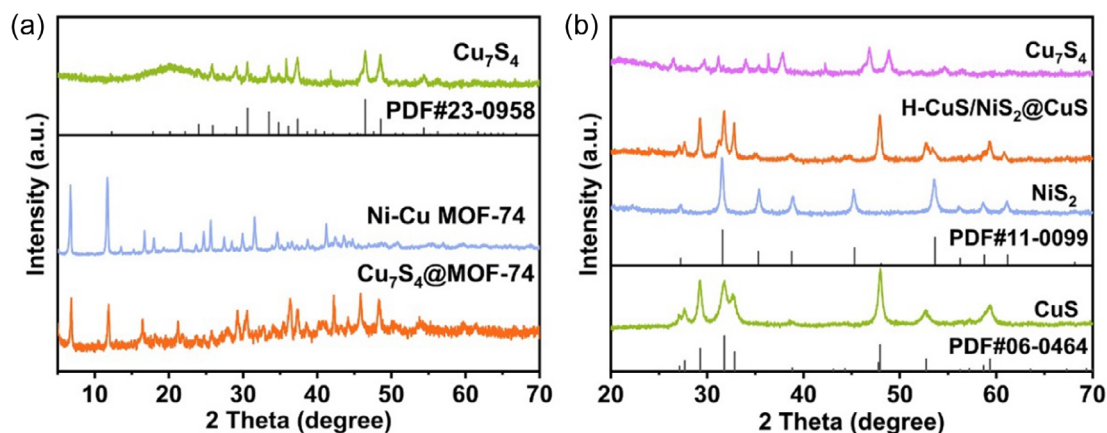


Figure 2. a,b) XRD pattern of samples.

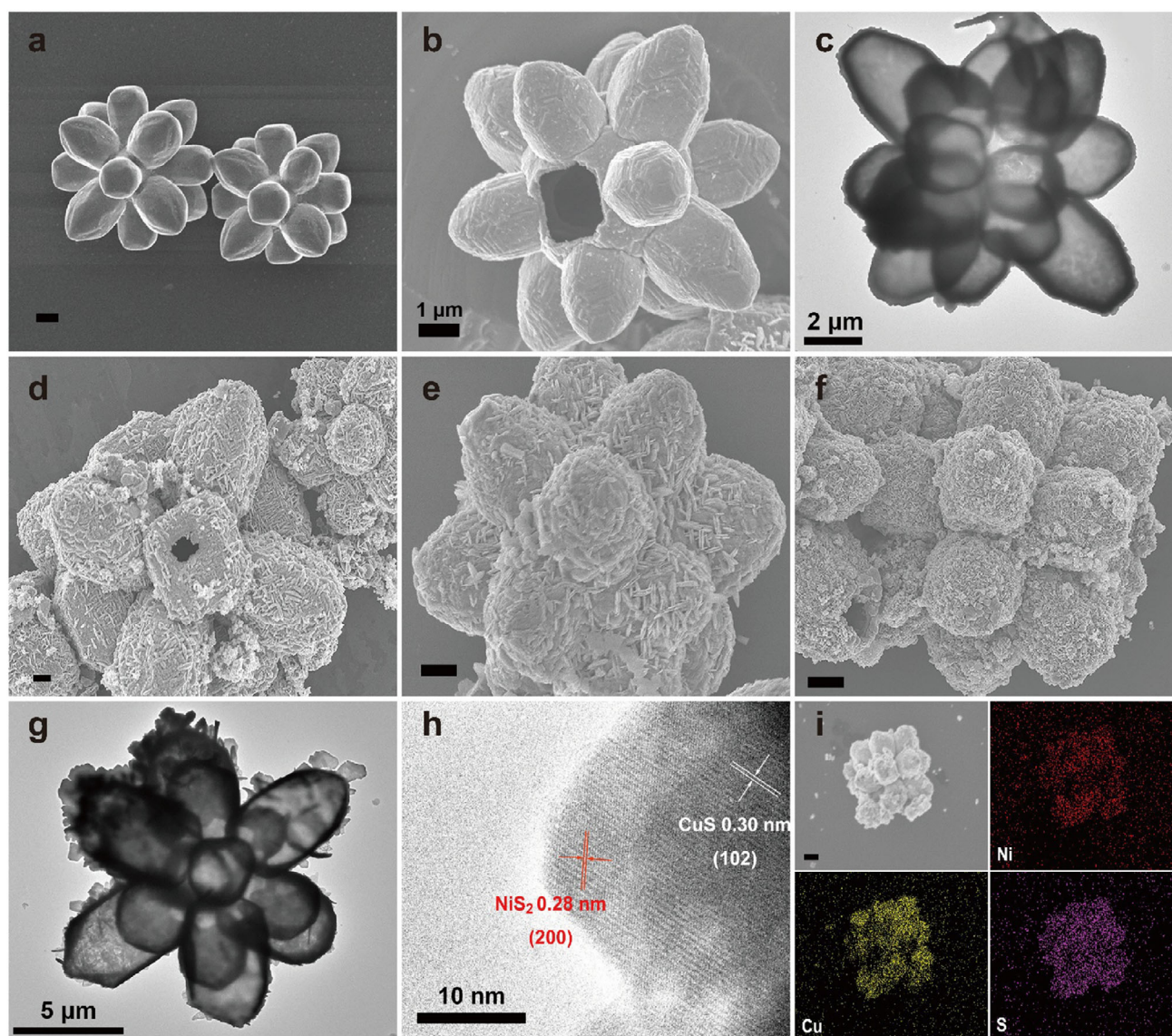


Figure 3. a) SEM image of  $\text{Cu}_2\text{O}$ . b) SEM image of hollow  $\text{Cu}_7\text{S}_4$ . c) TEM image of hollow  $\text{Cu}_7\text{S}_4$ . d,e) SEM image of  $\text{Cu}_7\text{S}_4/\text{Ni-Cu MOF-74}$ . f) SEM image of  $\text{H-CuS/NiS}_2@CuS$ . g) TEM image of  $\text{H-CuS/NiS}_2@CuS$ . h) HRTEM images of composites. Elemental mapping images of composites. i) EDS spectra of composite materials. The scale in figures (a,d,e,f, and i) is 1  $\mu\text{m}$ .



Scanning electron microscope (SEM), transmission electron microscopy (TEM), and energy dispersive spectrometer (EDS) were used to characterize the morphology, microstructure, and element distribution of the prepared photocatalysts. As illustrated in **Figure 3a**, the  $\text{Cu}_2\text{O}$  precursor had a 14-pod-like “succulent plant” shape, and its surface was vulcanized to form 14 pod-like  $\text{Cu}_7\text{S}_4$  shells. As can be seen from Figure 3b,c, the  $\text{Cu}_2\text{O}$  inside the  $\text{Cu}_7\text{S}_4$  will form a complex with  $\text{NH}_3$  to dissolve itself after soaking in ammonia water, thus forming a  $\text{Cu}_7\text{S}_4$  shell with a hollow structure. The bimetallic Ni-Cu MOF-74 was then grown on the hollow  $\text{Cu}_7\text{S}_4$  (Figure 3d,e). After sulfurization with thioacetamide, H-CuS/ $\text{NiS}_2$ @CuS composite material was formed with  $\text{NiS}_2$  and CuS nanosheets coated on the surface of hollow 14-pod CuS (Figure 3f,g). The microstructure of the material was further investigated by HRTEM. Figure 3h shows a clear interface between CuS and  $\text{NiS}_2$ . In addition, the 0.30 nm lattice spacing corresponds to the (102) crystal face of CuS.<sup>[29,30]</sup> And the 0.28 nm lattice spacing corresponds to the (200) crystal face of  $\text{NiS}_2$ .<sup>[31,32]</sup> Furthermore, the EDS spectrum (Figure 3i) shows that Cu, Ni, and S are uniformly distributed, which further indicates the successful synthesis of the H-CuS/ $\text{NiS}_2$ @CuS composite.

For the purpose of studying the constituents and valence states of the fabricated material, the H-CuS/ $\text{NiS}_2$ @CuS samples were analyzed by XPS. As can be seen from **Figure 4a**, XPS clearly shows the characteristic peaks of Cu 2p, S 2p, Ni 2p, and O 1s in the entire spectral range. As can be observed from the Figure 4b,c, following the formation of the composite material, the binding energy of the Cu and Ni elements undergoes a slight shift, which implies that there exists a powerful electronic interaction force between CuS and  $\text{NiS}_2$ . In the Ni 2p spectrum, there are two major peaks appearing at

853.40 and 870.84 eV, and these are in line with Ni 2p<sub>3/2</sub> and Ni 2p<sub>1/2</sub> for  $\text{Ni}^{2+}$ . The other two peaks, positioned at 855.34 and 874.19 eV, correspond to Ni 2p<sub>3/2</sub> and Ni 2p<sub>1/2</sub> of  $\text{Ni}^{3+}$ .<sup>[33,34]</sup> In addition, we also observed the satellite peak of Ni at 859.23 and 876.88 eV, and the spectrum shows that Ni mainly exists in the form of  $\text{Ni}^{2+}$  and  $\text{Ni}^{3+}$  valence. After the formation of the composite material, the binding energy of Ni element has a positive shift, indicating that the electron density on the surface of  $\text{NiS}_2$  is reduced, and the electrons are transferred out of  $\text{NiS}_2$ . In the XPS spectra of Cu 2p, two peaks whose binding energy were 931.76 and 951.74 eV are spotted, corresponding to Cu 2p<sub>3/2</sub> and Cu 2p<sub>1/2</sub> of  $\text{Cu}^{2+}$ , indicating that Cu exists in the valence form of  $\text{Cu}^{2+}$ .<sup>[35,36]</sup> After the formation of the composite material, the binding energy of the Cu element has a negative shift, indicating that the electron density on the surface of the H-CuS and CuS increases and electrons are transferred to them.<sup>[37,38]</sup> The early results show that after H-CuS, CuS, and  $\text{NiS}_2$  are combined, the electron density on the surface of the material changes, and the electrons are transferred from  $\text{NiS}_2$  to H-CuS and CuS. In addition, the S 2p spectrum shows two peaks, one at 163.34 eV and the other at 162.15 eV (Figure 4d), and these peaks correspond to S 2p<sub>3/2</sub> and S 2p<sub>1/2</sub> while the smaller peak at 168.87 eV belongs to the S=O bond, which results from the surface oxidation of the sulfide.<sup>[39,40]</sup> The aforementioned XPS analysis indicates that after the successful preparation of the composite, the electrons on  $\text{NiS}_2$  are transferred to H-CuS and CuS.

## 2.2. The Photocatalytic Performance of Materials

HER experiments were carried out using Eosin Y (EY) as the photosensitizer and triethanolamine as the sacrificial agent. Hydrogen

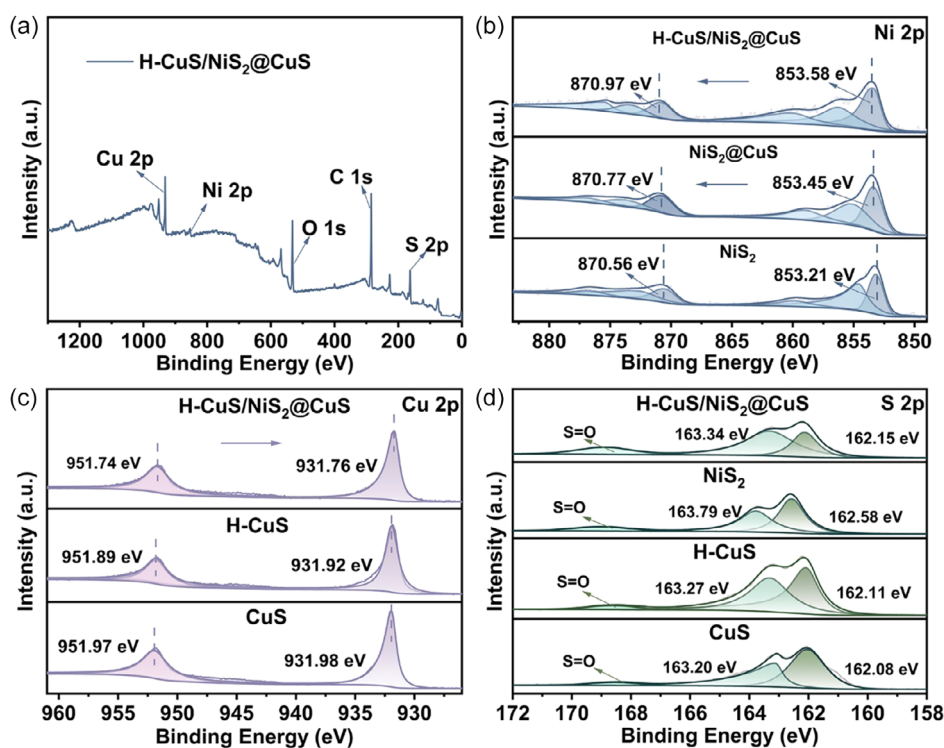


**Figure 4.** a) The XPS full spectra of H-CuS/ $\text{NiS}_2$ @CuS. b) Ni 2p XPS spectrum. c) Cu 2p XPS spectrum. d) S 2p XPS spectrum.

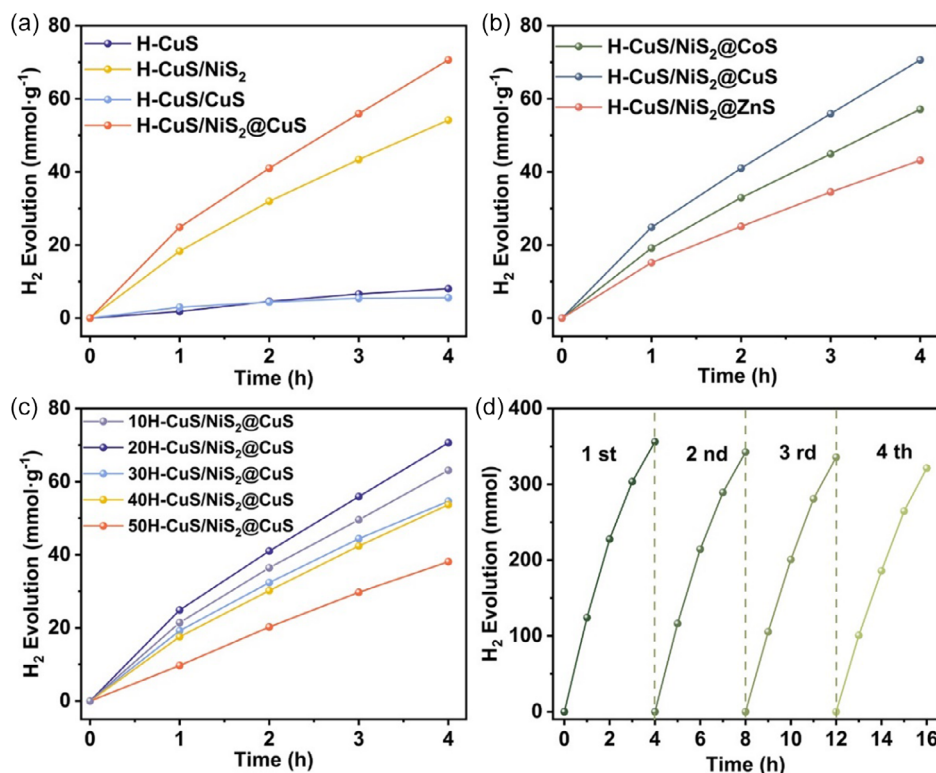


**Figure 5.** a) H<sub>2</sub> evolution rate of materials loaded with single metal MOF-74 after vulcanization. b) H<sub>2</sub> evolution rate of materials loaded with different bimetal MOF-74 (Ni-Cu MOF-74, Ni-Co MOF-74, Ni-Zn MOF-74) after vulcanization. c) H<sub>2</sub> evolution rate with different loads. d) Stability test of H-CuS/NiS<sub>2</sub>@CuS.

evolution experiments were performed under the condition of visible light ( $\lambda > 420$  nm) (Figure 5a). The rate at which H-CuS/NiS<sub>2</sub>@CuS evolves hydrogen can achieve 17.66 mmol g<sup>-1</sup> h<sup>-1</sup> (AQE = 6.77%,  $\lambda = 475$  nm), which is superior to that of H-CuS and the composite formed after vulcanization of single metal MOF-74. Then, we tested the composites after different bimetallic MOF-74 growing onto Cu<sub>7</sub>S<sub>4</sub> and vulcanization. It can be seen from Figure 5b that the composites formed by Ni-Cu bimetallic MOF-74 loading and vulcanization have the highest property in photocatalytic hydrogen evolution. Finally, we kept the content of MOF-74 unchanged, adjusted the proportion of different components of sulfide by changing the amount of Cu<sub>7</sub>S<sub>4</sub> matrix material, and tested its hydrogen evolution performance. As illustrated in Figure 5c, the property of the material in photocatalytic hydrogen evolution gradually improved as the amount of matrix material decreases, and the hydrogen evolution rate reached its maximum when the amount of Cu<sub>7</sub>S<sub>4</sub> was reduced to 20 mg. After four hydrogen production tests, the H-CuS/NiS<sub>2</sub>@CuS catalyst maintained a hydrogen production efficiency of 89% compared to the first cycle (Figure 5d), demonstrating the excellent photocatalytic hydrogen evolution stability of the composite.

UV-Vis DRS was utilized to investigate the band structure of the H-CuS/NiS<sub>2</sub>@CuS photocatalyst. As illustrated in Figure 6a, transition metal sulfides exhibit strong light absorption in the entire visible range. Compared with single sulfides, the visible light absorption rate of composite materials has been further improved, which is favorable for the photocatalytic HER. Furthermore, the bandgap of the material is further reckoned from the UV-Vis

DRS spectra of the semiconductor by means of the Kubelka-Munk approach.<sup>[41,42]</sup> As illustrated in Figure 6b–d, the bandgap values of H-CuS, CuS, and NiS<sub>2</sub> are 1.37, 1.31, and 1.47 eV, respectively. The bandgap value of H-CuS/NiS<sub>2</sub>@CuS is smaller than that of NiS<sub>2</sub> (Figure S3, Supporting Information), implying that the composite material is more readily excited by light and produces more photoinduced electrons and holes, enhancing the photocatalytic property of the material.

For the purpose of obtaining the band structure of the material, we performed Mott-Schottky tests on the synthesized materials, as illustrated in Figure 7a–c. The flat band potential ( $V_{FB}$ ) of H-CuS, CuS, and NiS<sub>2</sub> was calculated. The values are 1.72 V versus Ag/AgCl (=1.92 V versus NHE) for H-CuS, 1.67 V versus Ag/AgCl (=1.87 V versus NHE) for CuS, and -0.46 V versus Ag/AgCl (= -0.26 V versus NHE) for NiS<sub>2</sub>, respectively, indicating that H-CuS and CuS is a p-type semiconductor while NiS<sub>2</sub> is an n-type semiconductor. The valence band potential ( $V_{VB}$ ) of p-type semiconductors is typically raised by 0.1 to 0.2 V when compared to the flat band potential, and the conduction band potential ( $V_{CB}$ ) of n-type semiconductors is typically lower by 0.1 to 0.2 V when compared to the flat band potential. Consequently, the  $V_{VB}$  of H-CuS, CuS, and the  $V_{CB}$  of NiS<sub>2</sub> are respectively 2.02, 1.97, and -0.36 V (relative to NHE).<sup>[43–46]</sup> Therefore, the band structure of the material is illustrated in Figure 7d. The above test results in the Mott-Schottky chart indicate that NiS<sub>2</sub> presents a positive slope while H-CuS and CuS present a negative slope. These two materials have suitable band structures, and the construction of IEF can effectively separate e-h pairs. Furthermore, the charge

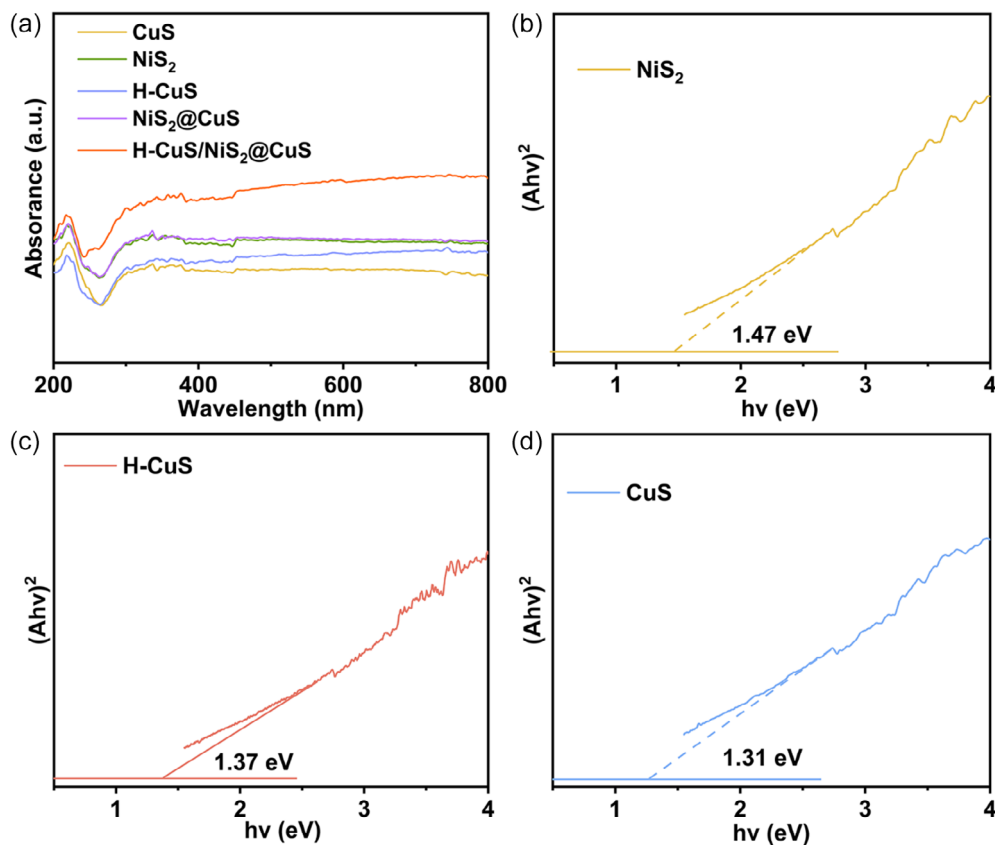


Figure 6. a) UV-Vis DRS spectra of samples. b–d) Optical bandgap for NiS<sub>2</sub>, H-CuS, and CuS. (The colored horizontal lines in (b–d) represent the baseline Y = 0).

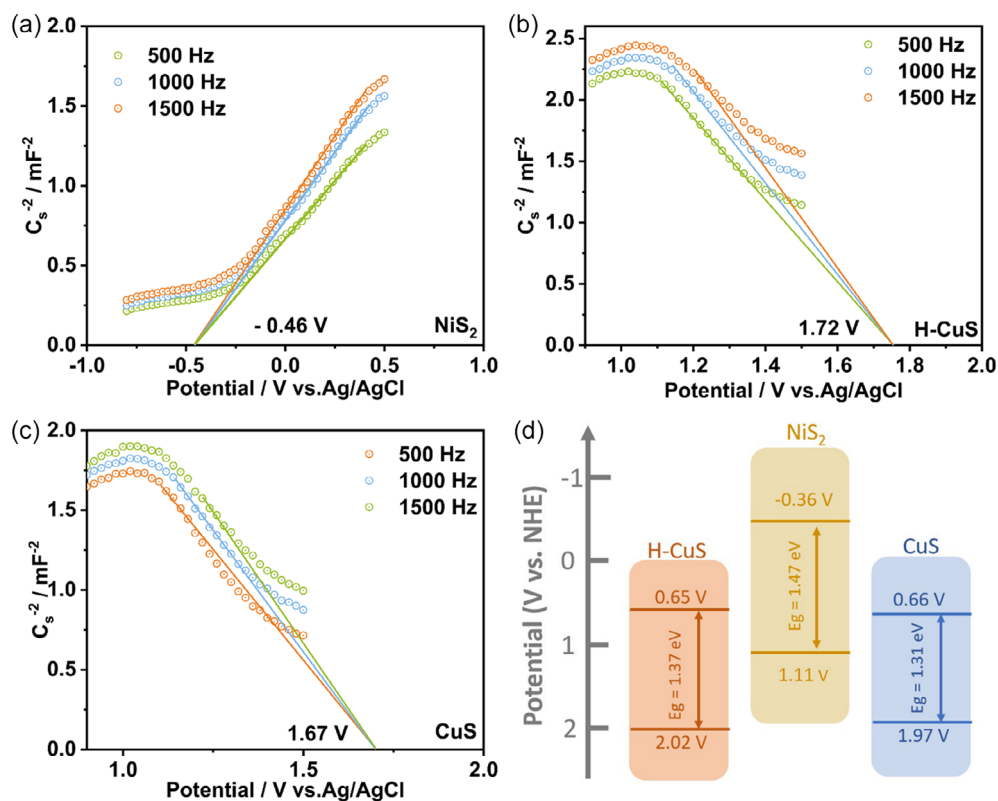
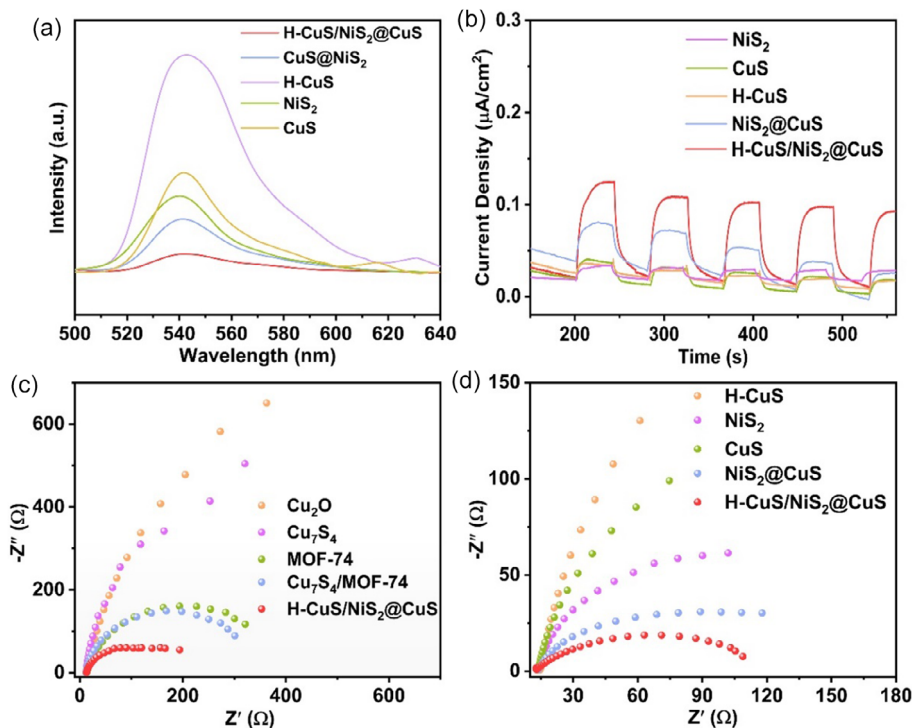


Figure 7. a–c) Mott–Schottky plots for NiS<sub>2</sub>, H-CuS, and CuS. d) Band structures for NiS<sub>2</sub>, H-CuS, and CuS.



**Figure 8.** a) PL spectra with EY. b) Response of transient photocurrent. c,d) Electrochemical impedance spectra of single sulfide, composite materials, and their precursors.

transfer mechanism is consistent with the S-scheme heterojunction, which makes photocatalytic HER proceed efficiently.

To study the separation ability of photoelectrons and holes in the photocatalyst, we tested the PL spectra of the material. As illustrated in **Figure 8a**, under the test conditions with an excitation wavelength of 380 nm, all the samples exhibit a distinct luminescence peak at 541 nm. A decrease in the intensity of the peak is indicative of an increased efficiency in the separation of e-h pairs, which also indicates a more favorable photocatalytic activity of the catalyst. It can be seen from the figure that the single sulfide has a strong luminescence peak, and the peak value of the composite obtained by vulcanizing Ni-Cu MOF-74 is significantly reduced, while the peak value of the composite obtained by vulcanizing bimetallic MOF-74 on  $\text{Cu}_7\text{S}_4$  is further reduced. The successful construction of heterojunction effectively separated the e-h pairs generated by photoexcitation. Among all the composite catalysts under investigation, H-CuS/ $\text{NiS}_2$ @CuS exhibits the lowest PL peak. This is in concordance with its optimal hydrogen production performance. It is further demonstrated that the formation of the H-CuS/ $\text{NiS}_2$ @CuS heterojunction is capable of diminishing the recombination of e-h pairs and substantially enhancing the hydrogen production property of the photocatalyst.

We monitored the variation of photocurrent density over time as illustrated in **Figure 8b**. It is observed that the transient photocurrent response of the composite is remarkably higher than that of the single sulfide. Among them, the H-CuS/ $\text{NiS}_2$ @CuS material has the maximum photocurrent density. This stronger response could be attributed to the close interaction between H-CuS, CuS, and  $\text{NiS}_2$ . This kind of interaction boosts charge transfer and lessens the recombination of e-h pairs. We used EIS to

investigate the charge transfer resistance. As illustrated in **Figure 8c,d**, the transition metal sulfide exhibited a relatively small impedance. The Nyquist plot for H-CuS/ $\text{NiS}_2$ @CuS shows the smallest semicircle, indicating that H-CuS/ $\text{NiS}_2$ @CuS has a smaller impedance than its precursors and single sulfide, which is favorable for photogenic charge transfer.

The mechanism of this photocatalytic process can be concisely recapitulated as follows:  $\text{NiS}_2$  is an n-type semiconductor, and H-CuS and CuS are p-type semiconductors, with significant differences in their Fermi levels. After the formation of the composite, electrons in  $\text{NiS}_2$  automatically have transferred to H-CuS and CuS due to the Fermi energy difference (**Figure 9a**). The outcomes are in line with the XPS analysis. Ultimately, their Fermi levels start to converge.<sup>[39,47]</sup> As illustrated in **Figure 9b**, the energy bands of H-CuS, CuS, and  $\text{NiS}_2$  are respectively bent due to the accumulation of electrons and the loss of electrons. Simultaneously, an internal electric field has been constructed at the interface of the composite materials.<sup>[44,48,49]</sup> After being exposed to visible light irradiation, the photocatalyst H-CuS/ $\text{NiS}_2$ @CuS is excited, resulting in the generation of electron-hole pairs. In virtue of the combined effects of band bending, IEF and Coulomb repulsion, some holes in the  $V_{\text{VB}}$  of  $\text{NiS}_2$  recombine with electrons in the  $V_{\text{CB}}$  of H-CuS and CuS under the influence of the IEF, leading to an assemblage of photoelectrons in the  $V_{\text{CB}}$  of  $\text{NiS}_2$  (**Figure 9c**). Consequently, the retained electrons within  $\text{NiS}_2$  exhibit a high reducing power and can catalyze the dissociation of water into hydrogen.<sup>[37,50]</sup> H-CuS and CuS amass a greater number of holes in  $V_{\text{VB}}$ , which considerably enhances the separation efficiency of e-h pairs. Electron transfer mechanism in this composite is in line with standard S-scheme heterojunction. Simultaneously, EY is photoexcited and transmuted into the excited state  $\text{EY}^*$ .

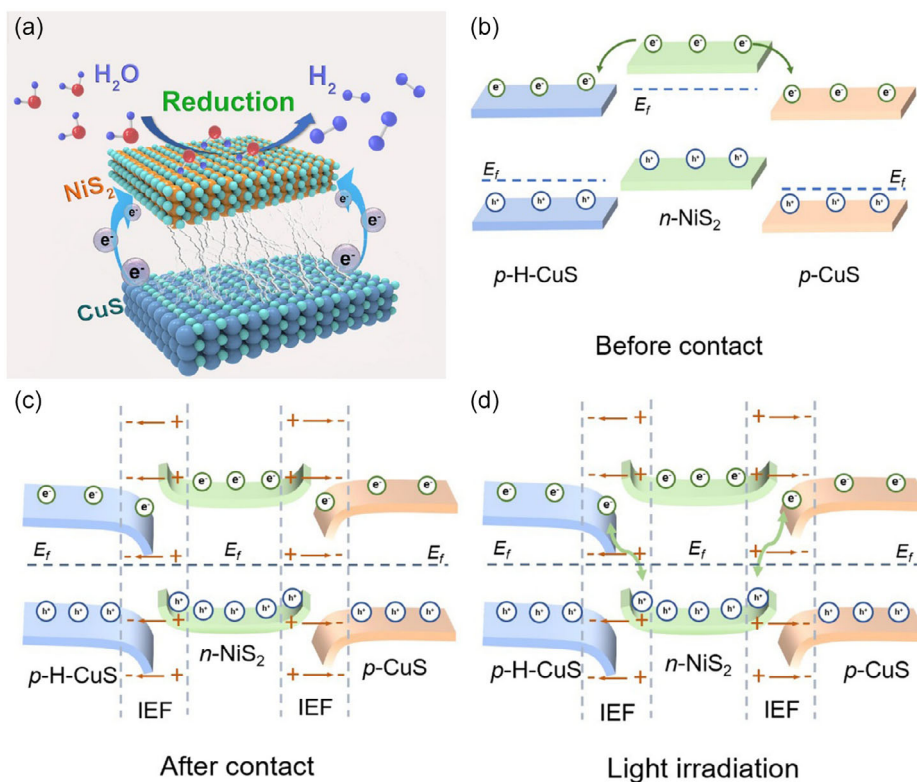


**Figure 9.** a) Diagram of photocatalytic water decomposition of a sample. b–d) The photocatalytic reaction mechanism of the samples.

Through intersystem crossing,  $EY^1^*$  is transformed into a more stable triplet excited state  $EY^{3*}$ .<sup>[51,52]</sup> The sacrificial agent TEOA captures the holes on the CuS, and TEOA is oxidized to  $TEOA^+$ , thus facilitating the conversion of  $EY^{3*}$  to  $EY^-$ .<sup>[53,54]</sup> The electrons generated by EY are transferred to the  $V_{CB}$  of  $NiS_2$ , which aggregates electrons on the  $V_{CB}$  of  $NiS_2$ .

### 3. Conclusion

In summary, bimetallic MOF-74 was grown on hollow  $Cu_7S_4$  by solvothermal method. Subsequently, after being vulcanized, the composite  $H-CuS/NiS_2@CuS$  was obtained.  $H-CuS/NiS_2@CuS$  demonstrates a superior level of activity in the photocatalytic of HER.  $H-CuS/NiS_2@CuS$  (20 mg base material) had the most excellent photocatalytic property of HER, and the hydrogen evolution rate reached  $17.66 \text{ mmol g}^{-1} \text{ h}^{-1}$ , significantly higher than that of single transition metal sulfide. The activity of HER was still high after 4 cycles. In addition, the test results show that  $H-CuS$  and  $CuS$  is a p-type semiconductor,  $NiS_2$  is an n-type semiconductor, and the electron transfer mechanism is consistent with that of S-scheme heterojunction. In the S-scheme heterojunction, the IEF causes photoelectrons to accumulate at the  $V_{CB}$  of  $NiS_2$ , which keeps  $NiS_2$  highly reducible in HER, effectively separating photogenerated electrons and hole pairs. This research offers a theoretical foundation for analyzing the principle of IEF in S-scheme heterojunctions and also opens up a new path for the construct of heterojunctions in the synthesis of highly active photocatalysts.

### Acknowledgements

This work was financially supported by the National Natural Science Foundation of China (no. 22271022) and the Science and Technology Development Planning of Jilin Province (no. YDZJ202201ZYTS342). This work was also supported by the China Scholarship Council (CSC No. 201802335014). Partial support from the Robert A. Welch Foundation (B-0027) (S.M.) and Saudi Water Authority through Energy Innovation Research Chair at Princess Nourah bint Abdulrahman University (T.A.) is also acknowledged.

### Conflict of Interest

The authors declare no conflict of interest.

### Data Availability Statement

The data that support the findings of this study are available from the corresponding author upon reasonable request.

**Keywords:** CuS · heterojunction · hollow structures ·  $NiS_2$  · photocatalytic hydrogen production

- [1] T. Takata, J. Jiang, Y. Sakata, M. Nakabayashi, N. Shibata, V. Nandal, K. Seki, T. Hisatomi, K. Domen, *Nature* **2020**, *581*, 411.
- [2] P. Zhou, M. Luo, S. Guo, *Nat. Rev. Chem* **2022**, *6*, 823.



- [3] Q. Zhou, Y. Guo, Y. Zhu, *Nat. Catal.* **2023**, *6*, 574.
- [4] X. Zhang, Y. Sun, S. Ju, J. Ye, X. Hu, W. Chen, L. Yao, G. Xia, F. Fang, D. Sun, X. Yu, *Adv. Mater.* **2023**, *35*, 2206946.
- [5] Y. Cao, S. Chen, S. Bo, W. Fan, J. Li, C. Jia, Z. Zhou, Q. Liu, L. Zheng, F. Zhang, *Angew. Chem., Int. Ed.* **2023**, *62*, e202303048.
- [6] H. Song, S. Luo, H. Huang, B. Deng, J. Ye, *ACS Energy Lett.* **2022**, *7*, 1043.
- [7] T. Hisatomi, K. Domen, *Nat. Catal.* **2019**, *2*, 387.
- [8] H.-T. Fan, Z. Wu, K.-C. Liu, W.-S. Liu, *Chem. Eng. J.* **2022**, *433*, 134474.
- [9] Y. Tang, Y. Sun, Y. Li, Y. Guo, B. Liu, X. Tan, Z. Hu, D. Zhong, J. Ye, T. Yu, *Adv. Funct. Mater.* **2024**, *34*, 2405527.
- [10] K. Yang, Y. Huang, T. Wang, Y. Li, Y. Du, J. Ling, Z. Fan, C. Zhang, C. Ma, *Adv. Mater.* **2024**, *36*, 2409832.
- [11] S. Liu, X. Guo, W. Wang, Y. Yang, C. Zhu, C. Li, W. Lin, Q. Tian, Y. Liu, *Appl. Catal., B* **2022**, *303*, 120909.
- [12] S. Chandrasekaran, L. Yao, L. Deng, C. Bowen, Y. Zhang, S. Chen, Z. Lin, F. Peng, P. Zhang, *Chem. Soc. Rev.* **2019**, *48*, 4178.
- [13] M. Dai, R. Wang, *Small* **2021**, *17*, 2006813.
- [14] M. Ding, S. Cui, Z. Lin, X. Yang, *Appl. Catal., B* **2024**, *357*, 124333.
- [15] G. M. Tomboc, B. T. Gadisa, J. Joo, H. Kim, K. Lee, *Chem. Nano. Mat.* **2020**, *6*, 850.
- [16] Z. Yu, X. Luan, H. Xiao, Y. Yang, D. Luo, J. Zi, Z. Lian, *Appl. Catal., B* **2024**, *347*, 123702.
- [17] Q. Li, K. Wu, P. Chen, H. Zhang, X. Bai, S. Yue, Z. Zhao, *Mater. Today Phys.* **2024**, *44*, 101439.
- [18] Y. Tong, Y. Hou, Z. Zhang, L. Yan, X. Chen, H. Zhang, X. Wang, Y. Li, *Appl. Catal., A* **2023**, *665*, 119387.
- [19] J.-E. Zhou, J. Chen, Y. Peng, Y. Zheng, A. Zeb, X. Lin, *Coordin. Chem. Rev.* **2022**, *472*, 214781.
- [20] G. Sun, Z. Tai, F. Li, Q. Ye, T. Wang, Z. Fang, L. Jia, W. Liu, H. Wang, *Small* **2023**, *19*, 2207758.
- [21] C. Q. Li, X. Du, S. Jiang, Y. Liu, Z. L. Niu, Z. Y. Liu, S. S. Yi, X. Z. Yue, *Adv. Sci.* **2022**, *9*, 2201773.
- [22] H. Zhang, Z. Zhang, B. Li, Y. Hua, C. Wang, X. Zhao, X. Liu, *CrystEngComm* **2015**, *17*, 3908.
- [23] T. Chen, F. Wang, S. Cao, Y. Bai, S. Zheng, W. Li, S. Zhang, S. X. Hu, H. Pang, *Adv. Mater.* **2022**, *34*, 2201779.
- [24] T. Chen, H. Xu, S. Li, J. Zhang, Z. Tan, L. Chen, Y. Chen, Z. Huang, H. Pang, *Adv. Mater.* **2024**, *36*, 2402234.
- [25] Y. Zhang, J.-D. Lu, G.-X. Zhang, R.-M. Zhu, H. Pang, *Rare Met.* **2023**, *43*, 478.
- [26] W. Liang, M. Wang, C. Ma, J. Wang, C. Zhao, C. Hong, *Small* **2023**, *20*, 2306473.
- [27] C. Karakaya, N. Solati, U. Savacı, E. Keleş, S. Turan, S. Çelebi, S. Kaya, *ACS Catal.* **2020**, *10*, 15114.
- [28] W. Shen, Y. Zheng, Y. Hu, J. Jin, Y. Hou, N. Zhang, L. An, P. Xi, C.-H. Yan, *J. Am. Chem. Soc.* **2024**, *146*, 5324.
- [29] Y. Li, Q. Zhao, Y. Zhang, Y. Li, L. Fan, F.-T. Li, X. Li, *Appl. Catal., B* **2022**, *300*, 120763.
- [30] Y. Xiao, D. Su, X. Wang, S. Wu, L. Zhou, Y. Shi, S. Fang, H. M. Cheng, F. Li, *Adv. Energy Mater.* **2018**, *8*, 1800930.
- [31] H. Liu, Q. He, H. Jiang, Y. Lin, Y. Zhang, M. Habib, S. Chen, L. Song, *ACS Nano* **2017**, *11*, 11574.
- [32] Q. Chen, S. Sun, T. Zhai, M. Yang, X. Zhao, H. Xia, *Adv. Energy Mater.* **2018**, *8*, 1800054.
- [33] W. Xu, R. Zhao, Q. Li, B. Sun, J. Wu, W. Zhong, Y. Gao, X. Nan, Q. Huang, Y. Yang, X. Li, N. Yang, Q. Zhang, *Adv. Energy Mater.* **2023**, *13*, 2300978.
- [34] X. Zhu, Z. Pan, Y. Liu, S. Kang, L. Wang, W. Lu, *J. Colloid Interface Sci.* **2023**, *629*, 22.
- [35] L. Zhou, S. Dai, S. Xu, Y. She, Y. Li, S. Leveneur, Y. Qin, *Appl. Catal., B* **2021**, *291*, 120019.
- [36] Q. Bai, M. Liang, W. Wu, C. Zhang, X. Li, M. Liu, D. Yang, W. W. Yu, Q. Hu, L. Wang, F. Du, N. Sui, Z. Zhu, *Adv. Funct. Mater.* **2022**, *32*, 2112683.
- [37] Y. Sun, R. Xiong, X. Ke, J. Liao, Y. Xiao, B. Cheng, S. Lei, *Sep. Purif. Technol.* **2024**, *345*, 127253.
- [38] Z. Liu, F. Jin, X. Li, P. Zhang, Z. Jin, *J. Mater. Sci. Technol.* **2024**, *188*, 131.
- [39] Z. Lei, X. Cao, J. Fan, X. Hu, J. Hu, N. Li, T. Sun, E. Liu, *Chem. Eng. J.* **2023**, *457*, 141249.
- [40] C.-W. Tsao, S. Narra, J.-C. Kao, Y.-C. Lin, C.-Y. Chen, Y.-C. Chin, Z.-J. Huang, W.-H. Huang, C.-C. Huang, C.-W. Luo, J.-P. Chou, S. Ogata, M. Sone, M. H. Huang, T.-F. M. Chang, Y.-C. Lo, Y.-G. Lin, E. W.-G. Diau, Y.-J. Hsu, *Nat. Commun.* **2024**, *15*, 413.
- [41] J.-M. Lin, Z.-B. Mei, C. Guo, J.-R. Li, Y. Kuang, J.-W. Shi, J.-J. Liu, X. Li, S.-L. Li, J. Liu, Y.-Q. Lan, *J. Am. Chem. Soc.* **2024**, *146*, 22797.
- [42] H. Dong, L. Fang, K. X. Chen, J. X. Wei, J. X. Li, X. Qiao, Y. Wang, F. M. Zhang, Y. Q. Lan, *Angew. Chem., Int. Ed.* **2024**, *64*, e202414287.
- [43] R. He, H. Liang, C. Li, J. Bai, *Colloids Surf.* **2020**, *586*, 124200.
- [44] M. Yang, K. Wang, Y. Li, K. Yang, Z. Jin, *Appl. Surf. Sci.* **2021**, *548*, 149212.
- [45] L. Ma, J. Xu, Z. Liu, Y. Liu, X. Liu, S. Xu, *J. Mater.* **2022**, *57*, 6734.
- [46] V. Soni, P. Singh, A. A. P. Khan, A. Singh, A. K. Nadda, C. M. Hussain, Q. Van Le, S. Rizevsky, V.-H. Nguyen, P. Raizada, *J. Nanostruct.* **2022**, *13*, 129.
- [47] S.-D. Wang, L.-Y. Huang, L.-J. Xue, Q. Kang, L.-L. Wen, K.-L. Lv, *Appl. Catal., B* **2024**, *358*, 124366.
- [48] Y. Wu, P. Zhu, Y. Li, L. Zhang, Z. Jin, *ACS Appl. Energy Mater.* **2022**, *5*, 8157.
- [49] F. Li, Z. Fang, Z. Xu, Q. Xiang, *Energy Environ. Sci.* **2024**, *17*, 497.
- [50] Z. Yu, C. Guan, X. Yue, Q. Xiang, *Chin. J. Catal.* **2023**, *50*, 361.
- [51] L. Yang, J. Huang, L. Shi, L. Cao, W. Zhou, K. Chang, X. Meng, G. Liu, Y. Jie, J. Ye, *Nano Energy* **2017**, *36*, 331.
- [52] T. Zhou, X. Han, W. Shen, F. Ji, M. Liu, Y. Song, W.-W. He, *Chin. Chem. Lett.* **2024**, 110415.
- [53] Y. Qin, L. Zhang, B. Yang, R. Hou, G. Fu, T. Huang, R. Deng, S. Zhang, X. Meng, *J. Colloid Interface Sci.* **2024**, *660*, 617.
- [54] W. Zhen, H. Gao, B. Tian, J. Ma, G. Lu, *ACS Appl. Mater. Interfaces* **2016**, *8*, 10808.

Manuscript received: March 20, 2025

Revised manuscript received: April 26, 2025

Version of record online: May 30, 2025